Low-temperature magnetic structure of UNiGe

A. Purwanto*
Los Alamos Neutron Scattering Center, Los Alamos National Laboratory, New Mexico 87545

V. Sechovský and L. Havela
Department of Metal Physics, Charles University, CZ-12116 Prague 2, The Czech Republic

R. A. Robinson, H. Nakotte, and Allen C. Larson
Los Alamos Neutron Scattering Center, Los Alamos National Laboratory, New Mexico 87545

K. Prokeš, E. Brück, and F. R. de Boer
Van der Waals Zeeman Institute, University of Amsterdam, Valckenierstraat 65, 1018 XE Amsterdam, The Netherlands
(Received 15 May 1995)

We report on the magnetic structure of single-crystalline UNiGe in its low-temperature commensurate antiferromagnetic phase. UNiGe crystallizes in the orthorhombic TiNiSi structure type with space group $Pnma$ and undergoes two magnetic transitions at 51 and 42 K. Our data, taken at 20 K, rule out both of the previously reported magnetic structures for the low-temperature phase, though we find an ordering vector $\mathbf{q}=(0,\frac{1}{2},\frac{1}{2})$ in agreement with the previous powder study of Murasik *et al.* [J. Phys. Condens. Matter **3**, 1841 (1991)]. We observe both domains of the single-**q** structure, and show that this is preferred over a 2-**q** structure. We extract a moment of $0.91\mu_B$ per U atom, and it is likely that the moment lies within the *b*-*c* plane in a collinear moment-density-wave configuration. However, out-of-plane moment components are allowed by symmetry and our best refinement gives noncollinear canting out of the plane by approximately 20°. This structure belongs to one of the two possible irreducible representations, and we discuss its relationship to a more conventional Shubnikov-group analysis.

I. INTRODUCTION

Systematic study of many U intermetallics, especially in UTX compounds (T=transition metal, $X=p$-electron element), has led to the suggestion that the magnetocrystalline anisotropy is directly related to the bonding anisotropy. As a rule, the moment directions are perpendicular to the shortest U-U distance.[1,2] UNiGe is one member of the large group of the UTX compounds crystallizing in the orthorhombic TiNiSi-type structure. The TiNiSi structure is the ordered variant of the $CeCu_2$ structure, which can in turn be considered a distortion of the hexagonal AlB_2 structure. For the TiNiSi structure, the nearest U-U distance has a slight zigzag along the *a* axis, and we therefore expect the U moments to lie in the *b*-*c* plane.[2] A number of authors have claimed antiferromagnetic order around 42 K,[3–6] but our recent neutron experiments have shown the occurrence of an additional incommensurate phase between 42 and 51 K.[7,8] Bulk high-field magnetization measurements show that *a* is the hard magnetic axis,[3] and therefore the moments should lie in the *b*-*c* plane. In addition, the low-temperature moment is $1.47\mu_B$ per f.u. at 35 T. Magnetic moments in the *b*-*c* plane of UNiGe have also been deduced from two previous neutron-diffraction experiments.[9,11] However, the detailed interpretations of these experiments are contradictory. Murasik *et al.*[9] claim collinear moments along the *b* axis[10] with a doubled magnetic unit cell in the *b*-*c* plane, while Kawamata *et al.*[11] derived a model with moments along the *c* axis but with identical magnetic and nuclear unit cells. This unsatisfactory situation motivated our neutron-diffraction experiment at LANSCE using a single crystal of UNiGe. This paper concentrates on the low-temperature magnetic structure below 42 K.

II. METHODS

The $2\times2\times1.6$ mm^3 single crystal of UNiGe, grown by a modified Czochralski tri-arc technique, is the same as the one used in previous neutron measurements[7] and in the determination of the $\mathbf{B}-T$ magnetic phase diagram.[12–14] The sample was sealed under a He atmosphere in a vanadium can which was mounted on the cold finger of a Displex closed-cycle refrigerator which in turn was mounted on the single crystal diffractometer (SCD) at LANSCE, the spallation neutron source at Los Alamos National Laboratory. A white beam of pulsed neutrons is scattered by the sample onto an area detector (25×25 cm^2; position-sensitive; ^{3}He gas-filled counter) and the wavelengths (0.5 – 5 Å) are determined by their time of flight from the source to the detector. In essence, SCD operates as a wavelength-dispersive neutron Laue camera. The data reported here were taken at 60 K in the paramagnetic and at 20 K in the low-temperature phase. The data were analyzed using the general structure analysis system[15] (GSAS) together with an additional FORTRAN program written specifically for this experiment. The magnetic refinements were all done on the 20 K data, with subtraction of the paramagnetic 60 K data set.

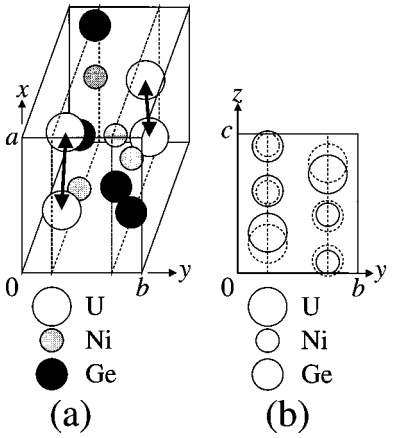

FIG. 1. The crystallographic structure of UNiGe shown as (a) a schematic unit cell and (b) its projection onto the *b*-*c* plane. The two mirror planes perpendicular to the *b* axis are shown as dashed lines: all atoms lie in these mirror planes. The nearest U-U distance $d_{\text{U-U}}$, shown as double-headed arrows in (a), has a slight zig-zag along the *a* axis. In (b), the atoms represented by the dashed-circles lie below those represented by full circles. The atoms are not drawn in scale but the positions within the unit cell are. The coordinate origin has been shifted by $(-0.25,0,0)$ with respect to the convention used in Table I.

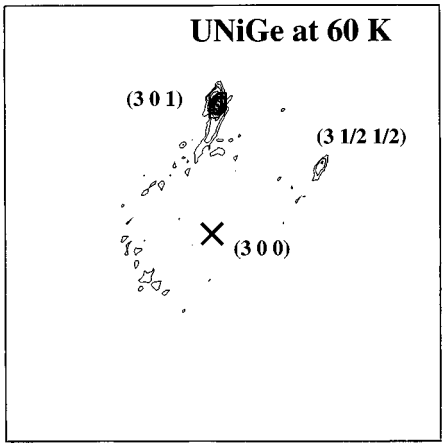

FIG. 2. Contour plot in reciprocal space of the 60 K data in the neighborhood of the (300) point. Note that we clearly see the $(3,1/2,1/2)$ reflection which is the (301) nuclear reflection of one of the twins described in the text. The data has been corrected for the incident spectrum and background has been subtracted.

III. RESULTS

A. Crystal structure and twinning

Using approximately 900 reflections observed in the paramagnetic phase at 60 K, we confirmed that UNiGe has the TiNiSi structure with the nonsymmorphic space group *Pnma*: the related space group *Imma* (disordered $CeCu_2$ structure type) can be excluded as we observe the (111), (112), (212), and (213) reflections, which violate the $h+k+l=2n$ selection rule for body-centered structures. Figure 1 shows (a) a schematic figure of the structure and (b) its projection onto the *b*-*c* plane. Each element occupies a $(4c)$-type site which has four equivalent positions in the unit cell.

In addition to the main Bragg reflections, we observed some extra weak reflections at $(h,k/2,l/2)$ positions. Although these additional peaks are weak, a rigorous analysis of their origin turned out to be indispensible for an understanding of the magnetism. For example, Fig. 2 shows a contour plot of some 60 K data in reciprocal space near the (300) point, where we find a noninteger reflection (3,1/2,1/2). A closer inspection of the whole 60 K data set indicates that all the extra reflections can be indexed as $(h,\pm k/2,\pm l/2)$. Based on the bulk measurements,[16] we know that the Néel temperature is 51 K. Hence, the appearance of the half-index-type reflections in the 60 K data cannot be of magnetic origin.

Note that TiNiSi structure type can be thought of as distortion of the hexagonal AlB_2 structure type and that the lattice constant *c* is very close to $\sqrt{3}b$ in the particular case of UNiGe. The extra reflections can be indexed as crystallites (or twins) rotated by 60° with respect to the main crystallite, as shown in Fig. 3. The $(h,\overline{1/2},1/2)$ and $(h,1/2,\overline{1/2})$ reflections can be indexed as $(h01)$ and $(h0\overline{1})$, repectively, in a twin rotated 60° counterclockwise around the *a* axis. Similarly, the $(h,1/2,1/2)$ and $(h\overline{1/2},\overline{1/2})$ peaks can be indexed as $(h01)$ and $(h0\overline{1})$ in a twin rotated 60° clockwise. Once this is done, the extra reflections index systematically as strong nuclear reflections in the TiNiSi structure, and those nuclear reflections that are weak or systematically absent are not observed. The volume fraction of each twin was found to be about 1% of the main crystallite. The refined structural parameters for the 60 K data are listed in Table I.

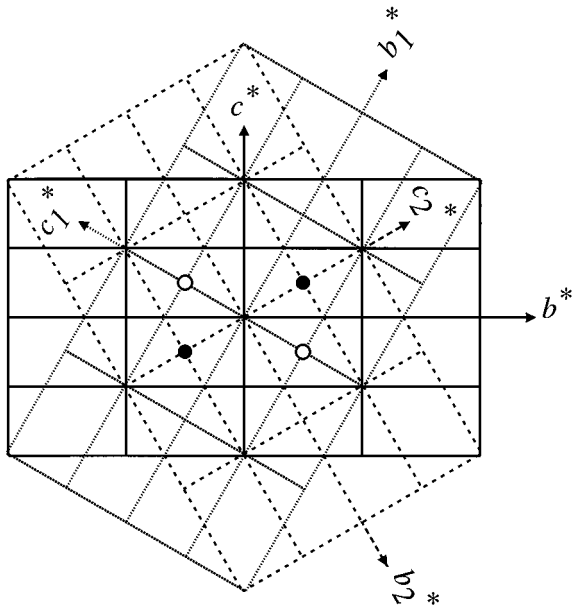

FIG. 3. Possible twinning of UNiGe at 60 K. The reciprocal lattice of the main grain is shown by the solid lines, while that of twin (1) is dotted and twin (2) is dashed. b^* and c^* are the reciprocal-lattice vectors for the main crystallite, while subscripts (1) and (2) belong to twins (1) and (2), which are observed at the 1% level, in our experiment. Twins (1) and (2) are rotated 60° counterclockwise and clockwise with respect to the main crystallite. The reflections denoted by the (○) and (●) symbols are indexed as $\pm(0,1/2,1/2)=\pm(001)_2$ and $\pm(0,1/2,1/2)=\pm(001)_1$, respectively.

TABLE I. Refined structural parameters for UNiGe at 60 K.

Space group *Pnma*					
U(4c)	x_U	0.25	z_U	$x_U = 0.0111 \pm 0.0001$	$z_U = 0.2054 \pm 0.0001$
Ni(4c)	x_{Ni}	0.25	z_{Ni}	$x_{Ni} = 0.3070 \pm 0.0001$	$z_{Ni} = 0.9193 \pm 0.0001$
Ge(4c)	x_{Ge}	0.25	z_{Ge}	$x_{Ge} = 0.7005 \pm 0.0001$	$z_{Ge} = 0.9088 \pm 0.0001$
Lattice parameters					
a(Å) = 6.9649 ± 0.0025					
b(Å) = 4.2452 ± 0.0022					
c(Å) = 7.1923 ± 0.0037					
Reduced $\chi^2 = 10.96$					

B. Magnetic structure

Figure 4 shows contour plots of representative data at 60 and 20 K. In total, we see 40 additional half-indexed reflections at 20 K which are presumably of magnetic origin, and from the main crystallite. The fact that the indices are non-integer immediately rules out Kawamata's structure;[11] our data show that the magnetic and crystallographic unit cells must have different sizes. All the extra reflections can be indexed assuming a wave vector $\mathbf{q} = (0,1/2,1/2)$. In Fig. 4(b), we show three peaks of the same multiplicity family, i.e., $(4,\underline{1/2},1/2)$, $(4,\underline{1/2},\underline{1/2})$, and $(4,1/2,\underline{1/2})$, while the $(4,1/2,1/2)$ peak lies outside the angular range of the detector. These reflections can be due either to two domains of a single-**q** magnetic structure or a 2-**q** magnetic structure with wave propagation vectors $\mathbf{q}_A = (0,1/2,1/2)$ and $\mathbf{q}_B = (0,1/2,1/2)$ as shown in Fig. 4(c). The 2-**q** structure would give identical intensities in all four reflections. We observe 40% less intensity in $(4,\underline{1/2},1/2)$ than in $(4,1/2,1/2)$, and can therefore immediately say that these peaks belong to about 40% domain *A* and 60% domain *B*, respectively. More precise values of the magnetic domain fractions are listed in Table VI. Figure 4(c) illustrates the expected magnetic reflections for the two domains around such an allowed nuclear reflection.

The next task is to determine whether the moment is purely along the *b* axis as proposed by Murasik [9,10] whose model is shown in Fig. 5. One of our observed strong reflections, $(0,3/2,1/2)$ shown in Fig. 6(b), is particularly sensitive to this question: it would be almost absent if the moment were parallel to the *b* axis. We can therefore rule out Murasik's structure in addition to Kawamata's.

In order to sort through other possible magnetic structures in a systematic way, we have chosen to use irreducible representation theory.[17] Representation theory is a technique to obtain the possible magnetic structures corresponding to the wave propagation vector **q**. This is achieved by considering the action on the magnetic moments of those crystallographic symmetry transformations which leave **q** invariant, along with the corresponding irreducible representations. There are eight symmetry elements in *Pnma*, but three are sufficient to generate the whole group: a screw axis in the *x* direction 2_{1x}, a screw axis in the *y* direction 2_{1y}, and an inversion center $\bar{1}$ which are located, respectively, at $(x,1/4,1/4)$, $(0,y,0)$, and $(0,0,0)$. The other five symmetries in *Pnma* (Ref. 18) can be obtained by multiplications of

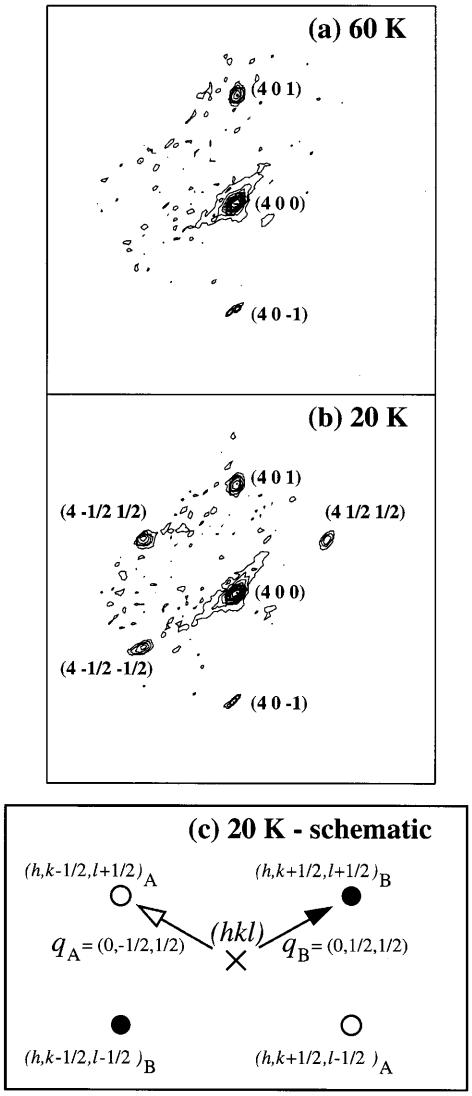

FIG. 4. Contour plot in reciprocal space in the neighborhood of the (400) reflection of (a) the 60 K data, (b) the 20 K data and (c) a schematic of the 20 K data. We see additional $(4,1/2,1/2)$, $(4,\underline{1/2},\underline{1/2})$ and $(4,1/2,\underline{1/2})$ magnetic reflections appear as the temperature is lowered. The $(4,1/2,1/2)$ reflection is outside the angular range of the detector. In (c), the magnetic contributions belonging to domain A (○) and domain B (●) around the (*hkl*) observed nuclear reflection (×) are shown. The data have been corrected for the incident spectrum and background has been subtracted.

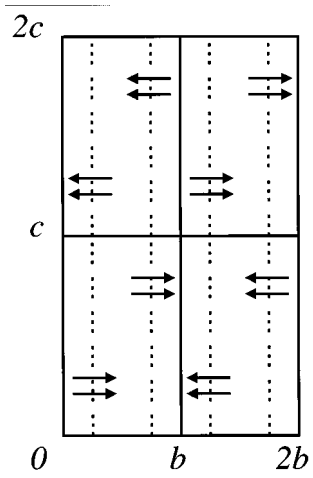

FIG. 5. The moment configuration in the *b*-*c* plane as proposed by Murasik *et al.* (Refs. 9 and 10). Four crystallographic cells are shown and the arrows represent the moment components in the *b*-*c* plane. The dotted lines indicate the crystallographic mirror planes perpendicular to the *b* axis. Note that this structure belongs to the $\Gamma^{(1)}$ representation (see below) with $\mu_x=\mu_z=0$.

these elements and are listed in Table II. Some of the symmetry elements project the atoms into a different unit cell. We then simply translate the atom back into the reference unit cell. This introduces a phase shift $\exp(i\mathbf{q}\cdot\mathbf{l})$ where $\mathbf{l}$ is a lattice translation vector. The effects of these symmetry elements on the moments are also listed in Table II. In order to obtain the irreducible representations, we transpose the transformation matrices corresponding to the symmetry elements. The transposition is needed in order to preserve the convention for the multiplication of group elements.[19] Furthermore, there is an anticommutation relation between $\widetilde{2_{1y}}\widetilde{\bar{1}}$ and $\widetilde{\bar{1}}\widetilde{2_{1y}}$:

$$\widetilde{2_{1y}}\widetilde{\bar{1}}=-\widetilde{\bar{1}}\widetilde{2_{1y}}, \tag{3.1}$$

where the tilde indicates matrix transposition. This is because the 2_{1y} and $\bar{1}$ symmetry elements anticommute with each other, once we include the $\exp(i\mathbf{q}\cdot\mathbf{l})$ phase shifts mentioned above. The existence of anticommutation indicates

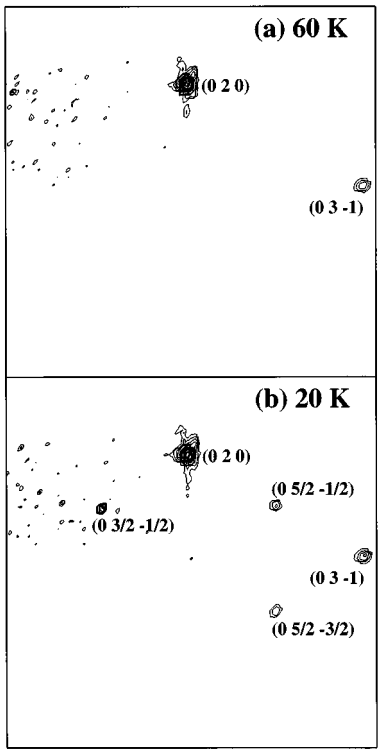

FIG. 6. Contour plot in reciprocal space of (a) the 60 K and (b) the 20 K data in the neighborhood of the $(020)\bar{}$ reflection. We see additional $(0,3/2,\bar{1}/2)$, $(0,5/2,\bar{1}/2)$ and $(0,5/2,\bar{3}/2)$ reflections appear as the temperature is lowered. The data have been corrected for the incident spectrum and background has been subtracted.

that the group elements cannot be represented by one-dimensional irreducible representations since one-dimensional representations always commute with each other.[20] We then use

$$\sum_i n_i^2=h, \tag{3.2}$$

where n_i is the dimension of *i*th irreducible representation and h is the order of the group which is the same as the number of symmetry elements in the group. There are no

TABLE II. Symmetry operations on moments for U atoms in the crystallographic unit cell as shown in Fig. 7.

	e	2_{1x}	2_{1y}	$\bar{1}$	$2_{1x}2_{1y}$	$2_{1x}\bar{1}$	$2_{1y}\bar{1}$	$2_{1x}2_{1y}\bar{1}$
μ_{1x}	μ_{1x}	μ_{4x}	μ_{3x}	μ_{3x}	μ_{2x}	μ_{2x}	$-\mu_{1x}$	μ_{4x}
μ_{2x}	μ_{2x}	μ_{3x}	$-\mu_{4x}$	μ_{4x}	$-\mu_{1x}$	μ_{1x}	μ_{2x}	$-\mu_{3x}$
μ_{3x}	μ_{3x}	μ_{2x}	$-\mu_{1x}$	μ_{1x}	$-\mu_{4x}$	μ_{4x}	μ_{3x}	$-\mu_{2x}$
μ_{4x}	μ_{4x}	μ_{1x}	μ_{2x}	μ_{2x}	μ_{3x}	μ_{3x}	$-\mu_{4x}$	μ_{1x}
μ_{1y}	μ_{1y}	$-\mu_{4y}$	$-\mu_{3y}$	μ_{3y}	μ_{2y}	$-\mu_{2y}$	μ_{1y}	μ_{4y}
μ_{2y}	μ_{2y}	$-\mu_{3y}$	μ_{4y}	μ_{4y}	$-\mu_{1y}$	$-\mu_{1y}$	$-\mu_{2y}$	$-\mu_{3y}$
μ_{3y}	μ_{3y}	$-\mu_{2y}$	μ_{1y}	μ_{1y}	$-\mu_{4y}$	$-\mu_{4y}$	$-\mu_{3y}$	$-\mu_{2y}$
μ_{4y}	μ_{4y}	$-\mu_{1y}$	$-\mu_{2y}$	μ_{2y}	μ_{3y}	$-\mu_{3y}$	μ_{4y}	μ_{1y}
μ_{1z}	μ_{1z}	$-\mu_{4z}$	μ_{3z}	μ_{3z}	$-\mu_{2z}$	$-\mu_{2z}$	$-\mu_{1z}$	$-\mu_{4z}$
μ_{2z}	μ_{2z}	$-\mu_{3z}$	$-\mu_{4z}$	μ_{4z}	μ_{1z}	$-\mu_{1z}$	μ_{2z}	μ_{3z}
μ_{3z}	μ_{3z}	$-\mu_{2z}$	$-\mu_{1z}$	μ_{1z}	μ_{4z}	$-\mu_{4z}$	μ_{3z}	μ_{2z}
μ_{4z}	μ_{4z}	$-\mu_{1z}$	μ_{2z}	μ_{2z}	$-\mu_{3z}$	$-\mu_{3z}$	$-\mu_{4z}$	$-\mu_{1z}$

TABLE III. Irreducible representations for $\boldsymbol{q}=(0,1/2,1/2)$.

	$\mathcal{E}$	$\widetilde{2}_{1x}$	$\widetilde{2}_{1y}$	$\widetilde{\widetilde{1}}$	$\widetilde{2}_{1x}\widetilde{2}_{1y}$	$\widetilde{2}_{1x}\widetilde{\widetilde{1}}$	$\widetilde{2}_{1y}\widetilde{\widetilde{1}}$	$\widetilde{2}_{1x}\widetilde{2}_{1y}\widetilde{\widetilde{1}}$
$\Gamma^{(1)}$	$\begin{pmatrix}1&0\\0&1\end{pmatrix}$	$\begin{pmatrix}-1&0\\0&-1\end{pmatrix}$	$\begin{pmatrix}0&1\\-1&0\end{pmatrix}$	$\begin{pmatrix}1&0\\0&-1\end{pmatrix}$	$\begin{pmatrix}0&-1\\1&0\end{pmatrix}$	$\begin{pmatrix}-1&0\\0&1\end{pmatrix}$	$\begin{pmatrix}0&-1\\-1&0\end{pmatrix}$	$\begin{pmatrix}0&1\\1&0\end{pmatrix}$
$\Gamma^{(2)}$	$\begin{pmatrix}1&0\\0&1\end{pmatrix}$	$\begin{pmatrix}1&0\\0&1\end{pmatrix}$	$\begin{pmatrix}0&1\\-1&0\end{pmatrix}$	$\begin{pmatrix}-1&0\\0&1\end{pmatrix}$	$\begin{pmatrix}0&1\\-1&0\end{pmatrix}$	$\begin{pmatrix}-1&0\\0&1\end{pmatrix}$	$\begin{pmatrix}0&1\\1&0\end{pmatrix}$	$\begin{pmatrix}0&1\\1&0\end{pmatrix}$

three-dimensional irreducible representations, because $3^2=9$ exceeds the order (8) of the group. We are left with two two-dimensional irreducible representations as $8=2^2+2^2$. After some straightforward but tedious algebra,[21] we obtain the irreducible representations $\Gamma^{(1)}$ and $\Gamma^{(2)}$ listed in Table III. Alternatively, one could use the irreducible representations tabulated elsewhere,[22] which are equivalent to those in Table III although the former are the two-dimensional complex irreducible representations.

By applying the projection operator method[17] to the results in Tables II and III, we obtain two basis vectors in each of $\Gamma^{(1)}$ and $\Gamma^{(2)}$ corresponding to the two domains *A* and *B* as shown in Table IV. The corresponding moment configurations are shown in Fig. 7. The essential physical difference between $\Gamma^{(1)}$ and $\Gamma^{(2)}$ is that the perpendicular moment components (per U atom in a given zig-zag chain along *a*) are ferromagnetically coupled within the chain in $\Gamma^{(1)}$ and antiferromagnetically coupled in $\Gamma^{(2)}$. Note that from the representation theory, all three Cartesian moment components are allowed. The moment magnitudes were deduced by least-squares refinement to the data with reasonable constraints on the moments, i.e., we expect the two domains to have the same magnetic anisotropy in relation to the parent crystal structure and thus $\theta_2=180°+\theta_1$ and $\phi_2=180°-\phi_1$ where the subscripts indicate domains. We use the spherical polar coordinate notation but with $0°\leqslant\theta\leqslant180°$ as the angle from the *a* axis and $0°\leqslant\phi\leqslant360°$ counterclockwise from the *b* axis in the *b*-*c* plane. After correcting for the Lorentz factor[23] and the U^{3+} magnetic form factor,[24] we find that $\Gamma^{(1)}$ is clearly preferred by the least-square refinement over $\Gamma^{(2)}$ (see Table V).

TABLE IV. Basis vectors corresponding to U atoms in the crystallographic unit cell as shown in Fig. 7.

Domain *A* of $\Gamma^{(1)}$	$\mu_{1x}-\mu_{2x}+\mu_{3x}-\mu_{4x}$
	$\mu_{1y}+\mu_{2y}+\mu_{3y}+\mu_{4y}$
	$\mu_{1z}+\mu_{2z}+\mu_{3z}+\mu_{4z}$
Domain *B* of $\Gamma^{(1)}$	$\mu_{1x}+\mu_{2x}-\mu_{3x}-\mu_{4x}$
	$\mu_{1y}-\mu_{2y}-\mu_{3y}+\mu_{4y}$
	$\mu_{1z}-\mu_{2z}-\mu_{3z}+\mu_{4z}$
Domain *A* of $\Gamma^{(2)}$	$\mu_{1x}-\mu_{2x}-\mu_{3x}+\mu_{4x}$
	$\mu_{1y}+\mu_{2y}-\mu_{3y}-\mu_{4y}$
	$\mu_{1z}+\mu_{2z}-\mu_{3z}-\mu_{4z}$
Domain *B* of $\Gamma^{(2)}$	$\mu_{1x}+\mu_{2x}+\mu_{3x}+\mu_{4x}$
	$\mu_{1y}-\mu_{2y}+\mu_{3y}-\mu_{4y}$
	$\mu_{1z}-\mu_{2z}+\mu_{3z}-\mu_{4z}$

There are two good physical reasons for believing that the moments might be confined to the *b*-*c* plane, and have no μ_x component. The first is the bulk magnetization result[3] mentioned in the introduction. The second is that $\Gamma^{(1)}$ with $\mu_x=0$ is a simple collinear moment-density-wave structure, with equal moments on all sites. In this case, the U atoms in the zig-zag chains are ferromagnetically coupled to each other. If all three components of the moments are allowed to vary, we obtain a reduced χ^2 of 2.33 and the moments are canted out of the *b*-*c* plane by approximately 20°. If we use the same $\Gamma^{(1)}$ model but with $\mu_x=0$, we obtain a reduced χ^2 of 2.71. However, our cross-section calculations reveal intensity differences between $\Gamma^{(1)}$ with $\mu_x=0$ and $\mu_x\neq0$ only in a number of rather weak reflections, which means that the present experiment is rather insensitive to the presence of the μ_x component. The reduced χ^2 for all models, including Murasik's model, are listed in Table V. As the $\Gamma^{(1)}$ with $\mu_x=0$ is simpler and more appealing on physical grounds, we list its magnetic parameters in Table VI.

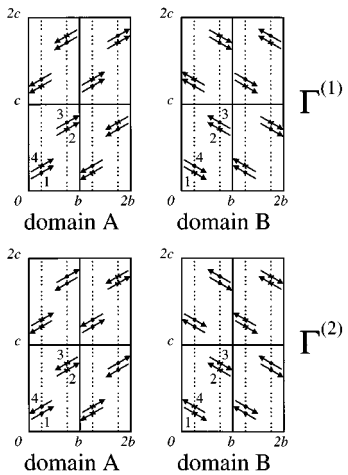

FIG. 7. Domains *A* and *B* corresponding to the $\Gamma^{(1)}$ irreducible representation and those of $\Gamma^{(2)}$. For the sake of clarity, only the moment directions of the U atoms are drawn. The U atoms in the first crystallographic unit cell are labeled 1, 2, 3, and 4. The arrows represent the moment components in a *b*-*c* plane. The dots and crosses represent the moment components parallel and antiparallel to the *a* axis, respectively. In the *b*-*c* plane, atoms 1 and 4 are ferromagnetically coupled for $\Gamma^{(1)}$ while those for $\Gamma^{(2)}$ are antiferromagnetically coupled. The dotted lines indicate the crystallographic mirror planes perpendicular to the *b* axis.

TABLE V. The reduced χ^2 for the magnetic refinements.

Model	Figure	U moment (μ_B)	Reduced χ^2
$\Gamma^{(2)}$	7	0.96 ± 0.01	6.56
$\Gamma^{(1)}$	7	0.96 ± 0.01	2.33
$\Gamma^{(1)}$ (with $\mu_x=0$)	7	0.91 ± 0.01	2.71
Murasik *et al.* (Refs. 9 and 10) ($\Gamma^{(1)}$ with $\mu_x=\mu_z=0$)	5	0.91 ± 0.01 [a]	5.17

[a]Murasik *et al.* (Ref. 9) obtained a U moment of $1.37\mu_B$ in their refinement.

IV. DISCUSSION

A. Consideration for the B−*T* phase diagrams

As shown above, we observe a small amount of crystallographic twinning, with twins related to the main crystallite by a 60° rotation. This observation may clear up a mystery concerning the $\mathbf{B}-T$ phase diagrams reported previously.[12]

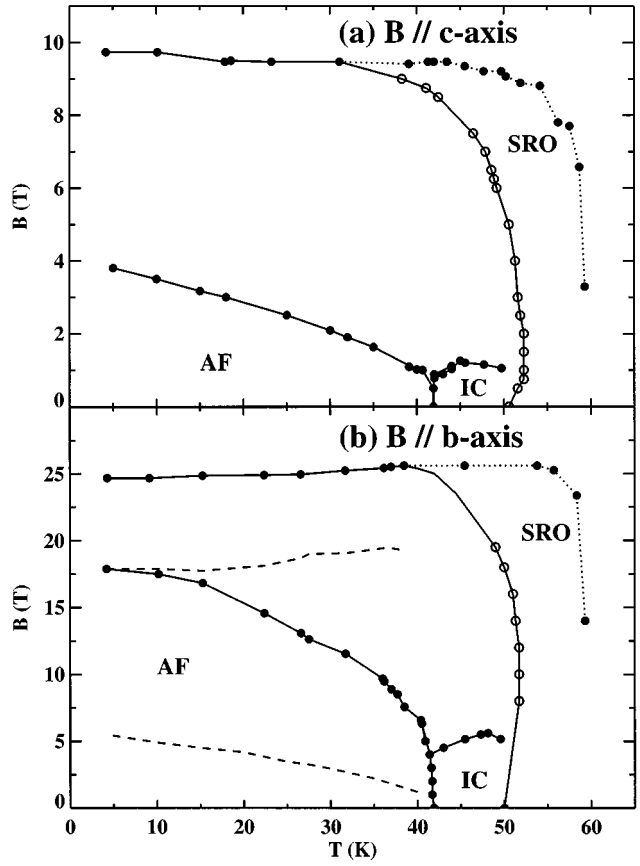

FIG. 8. Simplified magnetic phase boundaries from the detailed magnetic phase diagrams obtained by high-field magnetization (Refs. 12–14) for applied magnetic field along (a) the *c* axis and (b) the *b* axis. The solid circles were derived from magnetization data taken in field sweeps at constant temperature, while the open circles represent temperature sweeps at fixed field. There is also some evidence in the field sweeps for magnetic short-range order (SRO), but this was not observed in the temperature scans (Refs. 13 and 14). The antiferromagnetic and incommensurate phase are denoted as AF and IC, respectively. The dashed lines presumably arise from the crystallographic twins which see the magnetic field along the *b* axis of the main crystallite as a field 30° away from the *c* axis of the twins.

Using exactly the same crystal as in our study, de Boer *et al.*[12] determined the $\mathbf{B}-T$ phase diagrams for $\mathbf{B}\|b$ and $\mathbf{B}\|c$ by high-field magnetization at fixed temperatures. While the magnetization studies revealed two pronounced metamagnetic transitions for $\mathbf{B}\|c$, a far more complex magnetization behavior with up to four transitions for the *b*-axis was observed. de Boer's original data,[12] which were taken by sweeping the magnetic field at fixed temperatures, have since been supplemented by temperature scans[13,14] at fixed fields up to 20 T, and the resultant phase diagram is shown in Fig. 8. The two *b*-axis transitions shown by the dashed lines are very weak compared with the others,[12] and we now believe that they are not due to the main crystallite but due to the minority twins. The field in each minority twin is then much closer to the *c* axis (30° away to be precise) and the dashed lines reflect behavior intermediate between that of the ideal *b*-axis and ideal *c*-axis orientation.

B. Low-temperature and zero-field magnetic structure

In our structure, the resultant U moments are neither parallel nor perpendicular to the mirror planes of the crystallographic unit cell as one would expect in the magnetic (Shubnikov) space-group analysis, which suggests that the magnetic symmetry must be lower than the crystallographic symmetry. In fact, if one doubles the *b* and *c* axes as is necessary for $\mathbf{q}=(0,1/2,1/2)$, the smallest unit cell would be a monoclinic cell with eight U atoms. In principle, one would then expect a corresponding crystallographic struc-

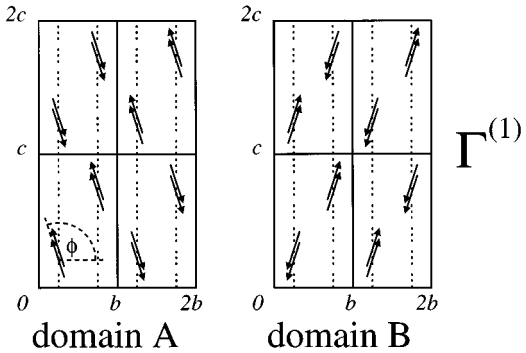

FIG. 9. The low-temperature magnetic structure of UNiGe consisting of two collinear antiferromagnetic domains corresponding to the $\Gamma^{(1)}$ representation. For the sake of clarity, only the moment directions of the U atoms are drawn. The arrows represent the moment components in the *b*-*c* plane. The dotted lines indicate the orthorhombic mirror planes perpendicular to the *b* axis.

TABLE VI. Refined magnetic parameters for UNiGe at 20 K supporting the moment configurations shown in Fig. 9.

	$\mu_x=0$	$\mu_x\neq 0$
Spherical polar coordinates with $0\leqslant\theta\leqslant 180°$ from the *a* axis and $0\leqslant\phi\leqslant 360°$ from the *b* axis in the *b*-*c* plane		
$\mu(\mu_B)$	0.91 ± 0.01	0.96 ± 0.01
$\theta(°)$	90.00 (fixed)	111.25 ± 0.83
$\phi(°)$	107.21 ± 1.83	108.60 ± 1.83
Cartesian coordinates		
$\mu_x(\mu_B)=\mu\cos\theta$	0.00 (fixed)	-0.35 ± 0.01
$\mu_y(\mu_B)=\mu\sin\theta\cos\phi$	-0.27 ± 0.01	-0.29 ± 0.01
$\mu_z(\mu_B)=\mu\sin\theta\sin\phi$	0.87 ± 0.01	0.85 ± 0.01
Fraction of domain *A* (%)	38.31 ± 0.71	38.87 ± 0.72
Reduced χ^2	2.71	2.33

tural distortion from orthorhombic to monoclinic. Within error bars, we were unable to detect any such structural distortion.

It is also interesting to compare our work with that on CaV_2O_4 which crystallizes in $Pnma$.[25] Note that the lattice parameters are interchanged with respect to our notation. Not only do the magnetic V atoms lie on the $4(c)$ sites, but the magnetic structure also has $\mathbf{q}=(0,1/2,1/2)$, as in UNiGe. These authors also used representation theory in deriving the possible magnetic structures. The irreducible representations and the basis vectors obtained are equivalent to ours with $\Gamma^{(1)}=\Gamma_{2k}$ and $\Gamma^{(2)}=\Gamma_{1k}$ where the right-hand sides are in their notation. After least-squares refinement, they obtained V moments pointing perpendicular to the crystallographic mirror planes although they noted the ambiguity of the fit from the two representations. This work was in agreemeent with the previous powder neutron diffraction work using the magnetic (Shubnikov) space group analysis in which the screw axis, glide plane, and mirror symmetry are preserved in the magnetic (monoclinic) unit cell.[26]

Now, our magnetic structure is also commensurate and can therefore also be categorized as one of the Shubnikov groups. To do this, we have to work in a larger monoclinic cell with eight U atoms per cell. One then loses the 2_{1y} (and the corresponding mirror plane) present in the parent $Pnma$ space group. The Shubnikov group for our magnetic structure is P_cb11 which is listed in the short-symbol notation with a unique *b* axis[27] as P_ac.

Finally, we note that the moment magnitude obtained in high-field measurements[3] at 4.2 K is $1.47\mu_B$/f.u., while that of the neutron data at 20 K is $0.91\mu_B$/U atom. This sort of discrepancy, which is not at all unusual in U intermetallics, cannot be attributed to the reduction of the $5f$ moment at higher temperatures alone. Unlike neutron diffraction, high-field magnetization tests the full bulk moment which could involve a non-negligible moment induced on the transition-metal sites.[28] Due to the complexity of the magnetic structure in the present case we did not try to refine an induced moment on the Ni sites. Moreover, application of a magnetic field can affect the degree of localization and a subsequent increase of the $5f$ moments with field as found for example in UCoAl.[29]

In conclusion, we believe that the magnetic structure of UNiGe is basically the collinear antiferromagnetic structure shown in Fig. 9 with a U moment of $0.91\mu_B$ confined in the *b*-*c* plane with both *y* and *z* components. Murasik's model[9,10] is, in fact, a simple case of ours: it also belongs to the $\Gamma^{(1)}$ representation but has $\mu_z=0$ in addition. Finally, our refinement throws up the interesting possibility that there are additional moment components perpendicular to the *b*-*c* plane, making the structure noncollinear.

ACKNOWLEDGMENTS

We are glad to acknowledge a number of helpful discussions with A. C. Lawson regarding the magnetic space group of the system. This work was sponsored by the U.S. Czechoslovak Science and Technology Joint Fund in cooperation with the MSMT CR and the U.S. Department of Energy under Project No. 93039. Also it was supported in part by the division of Basic Energy Sciences of the U.S. Department of Energy, by the Stichting voor Fundamenteel Onderzoek der Materie (FOM), and by the Grant Agency of the Czech Republic (Project No. 202/94/0454).

*Also at Physics Department, New Mexico State University, Las Cruces, NM 88003 and Material Science Research Center, National Atomic Energy Agency, Serpong, Tangerang 15310, Indonesia.

[1] V. Sechovský, L. Havela, H. Nakotte, F. R. de Boer, and E. Brück, J. Alloys Compounds **207/208**, 221 (1994).

[2] R. A. Robinson, A. C. Lawson, V. Sechovský, L. Havela, Y. Kergadallan, H. Nakotte, and F. R. de Boer, J. Alloys Compounds **213/214**, 528 (1994).

[3] L. Havela, V. Sechovský, F. R. de Boer, E. Brück, and H. Nakotte, Physica B **177**, 159 (1992).

[4] R. Troc and V. H. Tran, J. Magn. Magn. Mater. **73**, 38 (1988).

[5] K. H. J. Buschow, E. Brück, R. G. van Wierst, F. R. de Boer, L. Havela, V. Sechovský, P. Nozar, E. Sugiura, M. Ono, M. Date, and A. Yamagishi, J. Appl. Phys. **67**, 5215 (1990).

[6] S. Kawamata, R. Ishimoto, H. Iwasaki, N. Kobayoshi, Y. Yamaguchi, T. Komatsubara, G. Kido, T. Mitsugashira, and Y. Muto, J. Magn. Magn. Mater. **90-91**, 513 (1990).

[7] V. Sechovský, L. Havela, P. Svoboda, A. Purwanto, A. C. Larson, R. A. Robinson, K. Prokeš, H. Nakotte, F. R. de Boer, and H. Maletta, J. Appl. Phys. **76**, 6217 (1994).

[8] V. Sechovský, L. Havela, A. Purwanto, Allen C. Larson, R. A. Robinson, K. Prokeš, H. Nakotte, E. Brück, F. R. de Boer, P. Svoboda, H. Maletta, and M. Winkelmann, J. Alloys Compounds **213/214**, 536 (1994).

[9] A. Murasik, P. Fischer, R. Troc, and V. H. Tran, J. Phys. Condens. Matter **3**, 1841 (1991).

[10] Note that Murasik *et al.* (Ref. 9) used the $CeCu_2$ structure and *a* and *b* are interchanged with respect to the TiNiSi structure.

[11] S. Kawamata, K. Ishimoto, Y. Yamaguchi, and T. Komatsubara, J.

Magn. Magn. Mater. **104-107**, 51 (1992).
[12] F. R. de Boer, K. Prokeš, H. Nakotte, E. Brück, M. Hilbers, P. Svoboda, V. Sechovský, L. Havela, and H. Maletta, Physica **B 201** 251 (1994).
[13] H. Nakotte, L. Havela, V. Sechovsky, A. Lacerda, A. Purwanto, K. Prokeš, E. Brück, F. R. de Boer, and M. S. Torikachvili (unpublished),
[14] H. Nakotte (unpublished).
[15] A. C. Larson and R. B. Von Dreele, Los Alamos National Laboratory Report No. LA-UR-86-748.
[16] K. Prokeš, H. Nakotte, E. Brück, F. R. de Boer, L. Havela, V. Sechovský, P. Svoboda, and H. Maletta, IEEE Trans. Magn. **30**, 1214 (1994).
[17] J. Rossat-Mignod, in *Methods of Experimental Physics*, edited by Kurt Sköld and David L. Price (Academic, New York, 1987, Vol. 23, Part C, p. 112.
[18] *International Tables for Crystallography*, edited by T. Hahn (Kluwer, Dordrecht, 1987), Vol. A, p. 288.
[19] V. Heine, *Group Theory in Quantum Mechanics* (Dover, New York, 1993), p. 28.
[20] This is Schur's second lemma as discussed in standard group theory textbooks, see for instance, M. Hamermesh, *Group Theory and Its Application to Physical Problems* (Dover, New York, 1989), p. 101.
[21] E. F. Bertaut Acta Crystallogr. A **24**, 217 (1968).
[22] O. V. Kovalev, *Representations of the Crystallographic Space Groups: Irreducible Representations, Induced Representations and Corepresentations*, translated from Russian by G. C. Worthey, edited by H. T. Stokes and D. M. Hatch (Gordon and Breach, New York, 1993).
[23] G. E. Bacon, *Neutron Diffraction*, 3rd ed. (Oxford University Press, Oxford, England, 1975), p. 112.
[24] S. W. Johnson, R. A. Robinson, H. Nakotte, E. Brück, F. R. de Boer, and Allen C. Larson, J. Appl. Phys. **73**, 6072 (1993).
[25] E. F. Bertaut and N. V. Nhung, C. R. Acad. Sci. Ser. B **264**, 1416 (1967).
[26] J. M. Hastings, L. M. Corliss, W. Kunnmann, and S. La Placa, J. Phys. Chem. Solids **28**, 1089 (1967).
[27] See, for instance, C. J. Bradley and A. P. Cracknell, *The Mathematical Theory of Symmetry in Solids* (Oxford University Press, Oxford, England 1972), p. 588.
[28] J. A. Paixão, G. H. Lander, P. J. Brown, H. Nakotte, F. R. de Boer, and E. Brück, J. Phys. Condens. Matter **4**, 829 (1992).
[29] M. Wulff, J. M. Fournier, A. Delapalme, B. Gillon, V. Sechovský, L. Havela, and A. V. Andreev, Physica B **163**, 331 (1990).